IEEE Access
Multidisciplinary | Rapid Review | Open Access Journal

Received November 13, 2018, accepted February 24, 2019, date of publication March 18, 2019, date of current version April 12, 2019.

Digital Object Identifier 10.1109/ACCESS.2019.2905632

A Generalized Predictive Control-Based Path Following Method for Parafoil Systems in Wind Environments

JIN TAO[1,2], MATTHIAS DEHMER[3], GUANGMING XIE[2], (Member, IEEE), AND QUAN ZHOU[1], (Member, IEEE)

[1]Department of Electrical Engineering and Automation, Aalto University, 02150 Espoo, Finland
[2]College of Engineering, Peking University, Beijing 100871, China
[3]University of Applied Sciences Upper Austria, 4040 Steyr, Austria

Corresponding author: Jin Tao (jin.tao@aalto.fi)

This work was supported by the Academy of Finland under Grant 315660.

ABSTRACT Parafoil systems represent flexible wing vehicles. In case a vehicle is flying at low altitude, it is well known that the vehicle is more susceptible to winds. Also, due to the nonlinear, large inertial existing within the system, traditional control methods, such as traditional proportional-integral-derivative (PID), cannot guarantee the quality of path following. Therefore, we here apply generalized predictive control (GPC)-based method for parafoil systems to follow the designed path for a better control effect. To achieve this, we first propose a novel modeling method based on computational fluid dynamics to build a dynamic model of the parafoil system in windy environments. Afterward, a guidance law is designed according to a hybrid approach that combines the cross track error and the line of sight. In addition, the path following controller is established by using GPC. Finally, we generate and interpret numerical results to demonstrate the feasibility of the horizontal path following method in windy environments by utilizing the semi-physical simulation platform. The achieved results show that the GPC controller achieves high precision path following. More precisely, it possesses a better anti-wind ability and tracking accuracy and, therefore, the method outperforms PID controller.

INDEX TERMS Automatic control, modelling, parafoil system, wind environment, computational fluid dynamics, path following control, generalized predictive control.

I. INTRODUCTION

A parafoil system, composed of a traditional ram-air parafoil and a payload, is a unique kind of flexible vehicle. The perfect control and glide performance and large payload characteristics make it a practical platform for applications, e.g., equipment recovery and supplementary delivery. With the invention and development of Global Positioning System (GPS), Inertial Navigation System (INS), as well as micro control units, the implementation of fully autonomous path following methods and target hunting of the parafoil system become feasible [1]–[3].

The research on dynamic modeling of parafoil systems began with investigating three degree-of-freedom (DoF) models, of which the system was treated as a particle that usually used for path planning [4], [5]. Afterward, six DoF models, in which the parafoil and the payload were considered to be one rigid body have been developed [3], [6], [7]. Equally by accounting for relative motions between the parafoil and the payload, models with eight or nine DoF have been developed as well, see [8]–[10]. One can clearly see that the existing body of literature is mainly focused on mechanism modeling through force analysis of the parafoil-payload system [11]. Nonetheless, the study of wind effects on flight peculiarities are rather few, and the existing results only rely on a simple process of adding the wind speed into the speed of the parafoil, which is lack of theoretical fundaments.

For parafoil systems, flight control is realized by recycling steering ropes connected to both sides of the trailing edge of the parafoil canopy. The downward bending of the trailing edge changes the shape and orientation of its lifting surface

The associate editor coordinating the review of this manuscript and approving it for publication was Francesco Andriulli.

2169-3536 © 2019 IEEE. Translations and content mining are permitted for academic research only.
Personal use is also permitted, but republication/redistribution requires IEEE permission.
See http://www.ieee.org/publications_standards/publications/rights/index.html for more information.

and forms flaps and the deflection angle, such that the drag force increases and the yaw moment is produced, which leads the parafoil system turning to the recycling side [1]. For proving various disturbances existing in the actual environment, in case there is no proper controller to correct tracking errors, the parafoil system is unable to perform accurate path following. Therefore, control strategies are one of the key factors for path following control. In the following, we briefly survey related work. Benney *et al.* [2] has designed the traditional PD controller and the gain-scheduling fuzzy PD controller to realize the path following of parafoil systems. Slegers and Costello [12] applied the Model Predictive Control (MPC) method to control the parafoil system track the designed trajectory. Prakash and Ananthkrishnan [13] implemented a nonlinear dynamic inversion controller and showed the possibility of heading control. Jiao *et al.* [14] and Tao *et al.* [15], [16] tackled the problem of path following of parafoil systems by active disturbance rejection control (ADRC) and achieved some promising simulation and experimental results. Luo *et al.* [17] proposed a novel decoupling control approach using ADRC-based feedforward coupling compensation which proved evidence when it comes to strong tracking performance and robustness. Towards practical applications, the ALEX parafoil aerial delivery system developed by The Institute of Flight Systems of the German Aerospace Center (DLR), used a simple proportional controller [18]. Working on developing Guidance, Navigation & Control (GNC) algorithm for the Pegasus parafoil aerial delivery system, PID controllers have also been explored [19]. However, when asking for high performance, the PID control method has extensive bottlenecks to tackle these complicated systems [20].

In this paper, we apply Computational Fluid Dynamics (CFD) methods for analyzing the wind influences on aerodynamic performances of the parafoil canopy. Also, we develop a six DoF dynamic model of the parafoil system in windy conditions. In view of the nonlinear, large inertial within the system and strong winds in the actual environment, the Generalized Predictive Control (GPC) strategy perfectly adapts to the changing parameters and high order systems with random disturbances. The desired heading angle is obtained by the cross track error combined with the line of sight, and the controlled auto-regressive integrated moving average (CARIMA) model of the parafoil system is established through online identification by using recursive least squares method. The final semi-physical simulation results demonstrate the validity of the proposed controller.

The remainder of this paper is organized as follows: In Section II, we describe the dynamical model of the parafoil system in windy based on CFD. The GPC based path following control method of the parafoil system is discussed in Section III. The semi-physical simulation results are presented in Section IV. And we give a conclusion in Section V.

TABLE 1. Parafoil aerodynamic shape parameters.

Symbol	Quantity	Value
c	length of horizontal projection along the chord	3.18 m
b	length of horizontal projection along the span	10.62 m
R	length of chord	8.55 m
h	maximum distance form upper chord line to lower chord line along the span	0.36 m
β	lower contra-angle of the canopy	19.20 °
ε	half of central angle of the circular arc canopy	7 °

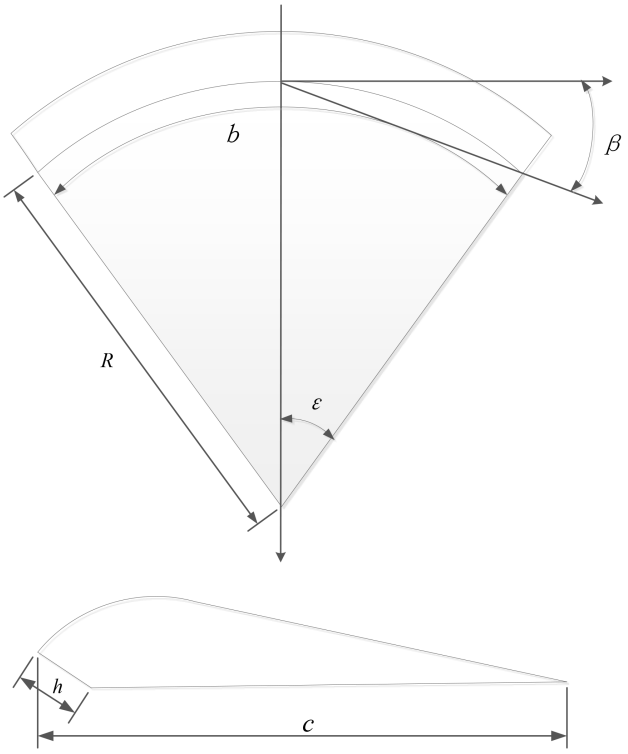

FIGURE 1. Aerodynamic shape of parafoil system.

II. DYNAMIC MODEL OF PARAFOIL SYSTEM

A. CFD SIMULATION OF PARAFOIL FLYING WITH WINDS

CFD is a branch of fluid mechanics that uses numerical analysis and data structures to solve and analyze problems involving fluid flows [22]–[24]. In this section, we use mesh velocity to simulate the wind filed, and dynamic mesh to simulate the attitude of parafoil, simulate and analyze the changing rules of the parafoil aerodynamic performance in the wind environments. The parameters of the aerodynamic shape of the CFD parafoil model are listed in Table 1.

When the sustained wind of speed v_w acting upon the parafoil canopy, the wind can be simulated by the moving mesh speed -v_w, The pitching and rolling motions of the parafoil are simulated by dynamic meshes generated by the smoothing method combined with the remeshing method. As shown in Fig.2, P stands for the pitch center, R denotes the roll center, O is the mass center of the parafoil system and T_w denotes the equivalent action-point of the wind.

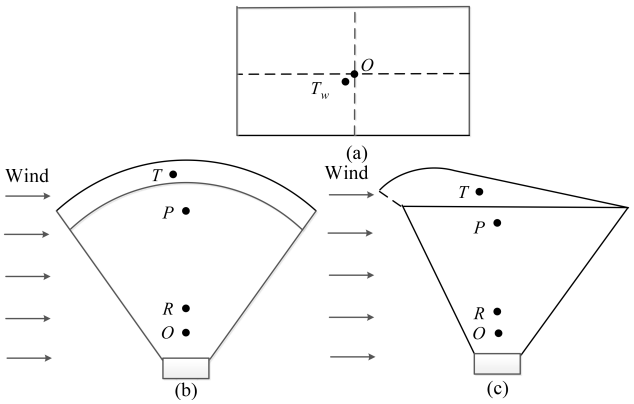

FIGURE 2. Schematic diagram of wind acting on paraofoil. (a) Top view. (b) Front view. (c) Side view.

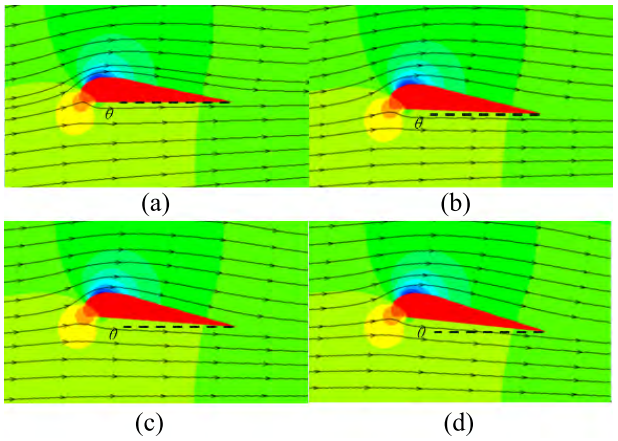

FIGURE 3. Pitch attitude of the parafoil in the wind environment. (a) $t = 5.0$s. (b) $t = 5.0$s. (c) $t = 8.3$s. (d) $t = 9.8$s.

To observe the attitude changing of the parafoil in winds, we add the sine wind with maximum speed of 5 m/s into the simulation environment during 5 s to 15 s. The simulation results are shown in Fig.3. We can see that at 6.6 s, the pitch angle of the parafoil θ equals 1.84°; at 8.3 s, θ equals 3.77°; and at 9.8 s, θ equals 5.70°. Therefore, the wind makes the parafoil canopy to pitch upward, which degree highly depends on the speed, the attack and the sideslip angle of the wind.

Then, we simulate the impact of winds on the parafoil aerodynamic with different wind speeds of 3 m/s, 5 m/s and 7 m/s. As shown in Fig. 4, the lift coefficient Cl and the drag coefficients Cd of the parafoil have the same change trend with the wind. As wind speeds are 3 m/s, 5 m/s and 7 m/s, the peak values of Cl are 1.214, 1.448 and 1.749, respectively; while the peak values of Cd are 1.214, 1.448 and 1.749, respectively. The wind causes the lift and drag forces of the parafoil increasing sharply, the variation range of which is proportional to the speed of the wind, and the change of velocity and attitude as well.

As mentioned before, the attack and the sideslip angle of the wind also affects the pitch and roll motion of the parafoil. Therefore, we perform simulations under the condition of the

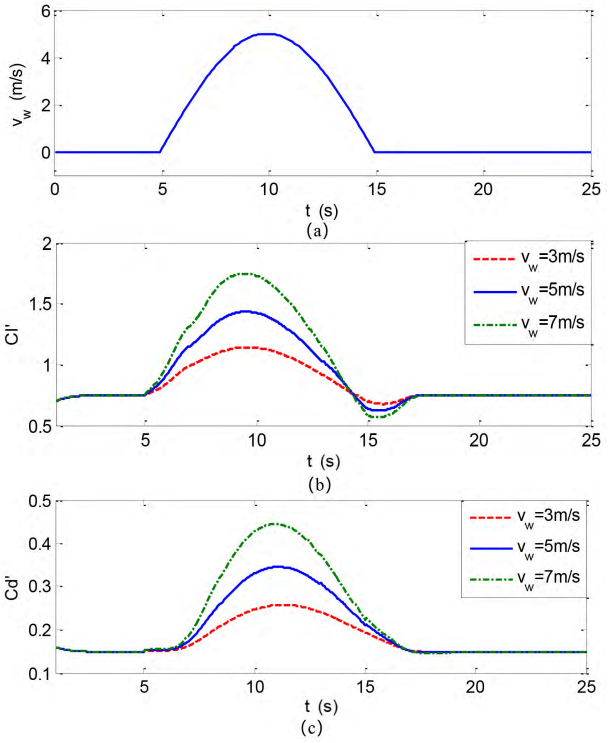

FIGURE 4. The impacts of wind on parafoil aerodynamic coefficients. (a) Wind of speed 5 m/s. (b) Lift coefficient. (c) Drag coefficient.

TABLE 2. Equivalent action points of the wind.

Attack angle of airflow	Equivalent action point T_x/c	Sideslip angle of airflow	Equivalent action point T_x/b
0	0.713	0	0.500
3	0.709	3	0.497
6	0.706	6	0.494
9	0.702	9	0.492
12	0.698	12	0.489
15	0.695	15	0.486
18	0.691	18	0.483

attack and the sideslip angle of the airflow changing from 0° to 18° with interval 3°. The equivalent action points of the wind are shown in Table 2. We observe that the equivalent action point moves backward in the tangential direction with the increase of the attack angle; and with the increase of the sideslip angle, the equivalent action point in the spanwise direction moves to the windward.

To summarize, by simulating parafoil flying in windy conditions through CFD, the equivalent forces and action points of winds can be obtained, which could serve as a foundation for modeling the parafoil system in the wind environment.

B. DYNAMIC EQUATIONS OF PARAFOIL SYSTEMS IN WINDS

In this section, we regard the parafoil and the payload to be a rigid connection. In consideration of the apparent mass of the parafoil and according to the Kirchhoff motion equation [8], we describe the six DoF dynamic model of the parafoil

system as follows:

$$\begin{bmatrix} \dot{v} \\ \dot{w} \end{bmatrix} = \begin{bmatrix} A_{11} & A_{12} \\ A_{21} & A_{22} \end{bmatrix}^{-1} \begin{bmatrix} F \\ M \end{bmatrix} \tag{1}$$

$$A_{11} = m_r + m_a \tag{2}$$

$$A_{22} = I_r + I_a - L^{\times}_{o-p} m_a L^{\times}_{o-p} \tag{3}$$

$$A_{12} = -A^T_{21} = -m_a L^{\times}_{o-p} \tag{4}$$

$$F = F_{aero} + F_g + F_{mex} + F_{aex} \tag{5}$$

$$M = M_{aero} + M_{mex} + M_{aex} \tag{6}$$

where $\dot{v}$ and $\dot{\omega}$ denote the acceleration and the angular acceleration of the parafoil system using the geodetic coordinate system. A_{11} is the sum of the real and the apparent mass respect to the mass center, A_{11} is the combination of the real and the apparent inertial, and A_{12} and A_{21} are the coupling of velocity and moment. $L^{\times}_{o-p}$ denotes the rotation matrix from the mass center to the apparent mass center. F denotes the total force acting upon the parafoil system, including the coupling forces of real mass F_{mex}, the apparent mass F_{aex}, the aerodynamic force F_{aero}, and gravity F_g. M denotes the total moment, including the apparent mass M_{aex}, the aerodynamic moment M_{aero} and the coupling forces of real mass M_{mex}. The calculation of F_g, F_{mex}, F_{aex}, M_{mex}, and M_{aex} are more complete [3], [6]. However, computing of F_{aero} and M_{aero} are a bottleneck in the parafoil system modeling.

We use a segmentation method to calculate the aerodynamic force of the parafoil canopy [6]. For this, we divide the canopy into eight distributed segments along the spanwise direction. The total aerodynamic force and torque of the parafoil yield to:

$$F_{aero} = \sum_{i=1}^{8} TR_{i-o} \left(F_{Li} + F_{Di}\right) + F_w \tag{7}$$

$$M_{aero} = \sum_{i=1}^{8} L^{\times}_{o-i} TR_{i-0} \left(F_{Li} + F_{Di}\right) + L^{\times}_{o-w} F_w \tag{8}$$

$$TR_{i-o} = \begin{bmatrix} 1 & 0 & 0 \\ 0 & \cos\gamma_i & \sin\gamma_i \\ 0 & -\sin\gamma_i & \cos\gamma_i \end{bmatrix} \tag{9}$$

$$F_{Li} = 0.5 C_L \rho S \left|v_i\right| \begin{bmatrix} v_{zi} & 0 & -v_{xi} \end{bmatrix}^T \tag{10}$$

$$F_{Di} = -0.5 C_D \rho S \left|v_i\right| \begin{bmatrix} v_{xi} & v_{yi} & v_{zi} \end{bmatrix}^T \tag{11}$$

where $i = 1, 2, \cdots, 8$ denotes the segment number, $L^{\times}_{o-i}$ and $L^{\times}_{o-w}$ is defined equally than $L^{\times}_{o-p}$. TR_{i-o} denotes the transformation matrix from the local coordinate of segment i of the canopy to the body coordinate determined by the rotating angle γ_i around the axis x_i. C_L and C_D denote the lift and drag coefficients, respectively. FL_i and FD_i denote the lift and drag forces of segment i, respectively, and F_w denotes the equivalent force of the wind. ρ denote the air density, S means the characteristic area of each segment, and v_i means the velocity of segment i in the body coordinate. The previous CFD simulation is mainly reflected in the calculation of $L^{\times}_{o-w}$ and F_w.

III. GPC BASED HORIZONTAL PATH FOLLOWING METHOD

The heading guidance and controller are two key elements in horizontal path following of the parafoil system. According to the horizontal deviation between the current position and the designed path of the parafoil, its desired heading is provided. As the heading of the parafoil system is manipulated through its heading controller, the vehicle will follow the designed path.

A. GUIDANCE LAW

In order to minimize the path following error, the guidance law is designed based on the hybrid approach that combines the cross track error and the line of sight [21]. Fig.5 shows the horizontal path following schematic of the parafoil system. Now we describe the calculation method of the path following error.

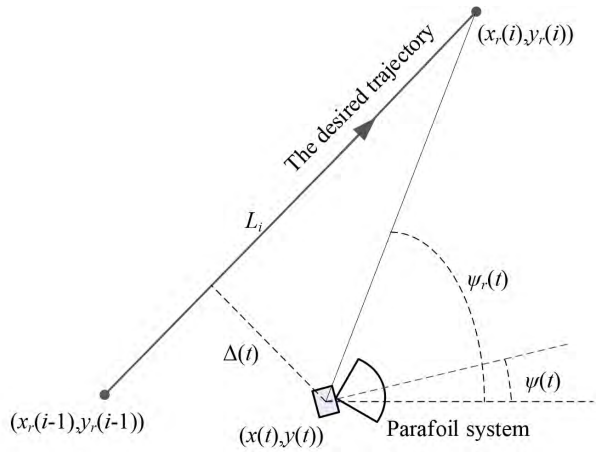

FIGURE 5. Horizontal path following scheme.

In Fig. 5, $(x(i), y(i))$ and $(x(i-1), y(i-1))$ denote the current and former desired trajectory target points, respectively. Also $(x(t), y(t))$ denotes the current position of the parafoil system.

Let's define:

$$\begin{cases} \Delta x = x_r(i) - x_r(i-1) \\ \Delta y = y_r(i) - y_r(i-1) \\ \hat{x} = x_r(i) - x(t) \\ \hat{y} = y_r(i) - y(t) \end{cases} \tag{12}$$

The distance between $(i-1)$-th and i-th trajectory points is given by:

$$L_i = \sqrt{\Delta x^2 + \Delta y^2}. \tag{13}$$

The path following error $\Delta(t)$ yields to:

$$\Delta(t) = \left(\hat{x}\Delta y - \hat{y}\Delta x\right) / L_i. \tag{14}$$

The heading angle of the desired trajectory is expressed by:

$$\psi_r(t) = \tan^{-1}(\Delta y / \Delta x). \tag{15}$$

According the trajectory tracking error and the heading angle of the setting trajectory, the heading angle tracking error $\psi_e(t)$ is given by:

$$\psi_e(t) = k_\Delta \Delta(t) + k_\psi(\psi_r(t) - \psi(t)). \tag{16}$$

where k_Δ and k_ψ are weighting coefficients, the values of which are assigning as:

$$\begin{cases} k_\Delta = \begin{cases} 0, |\psi_r - \psi| \geq |\psi_0| \\ k_1, |\psi_r - \psi| < |\psi_0| \end{cases} \\ k_\psi = \begin{cases} k_2, |\psi_r - \psi| \geq |\psi_0| \\ 0, |\psi_r - \psi| < |\psi_0| \end{cases} \end{cases} \tag{17}$$

where k_1, k_2, and ψ_0 are predefined constant. If the course deviation is large, the heading error is applied to reduce $\psi_e(t)$, whereas the trajectory tracking error is used.

B. GPC CONTROLLER DESIGN

GPC was firstly proposed by Clarke *et al.* [25], [26] in 1987 and is considered as a fundamental adaptive control algorithm. By keeping the online identification, output prediction and minimum variance control of minimum variance self-tuning control, and absorbing optimal rolling strategy, it inherits the performances of both the adaptive control and predictive control. And nowadays, the GPC has become one of the most potent and useful model-based control methods for a broad class of complex dynamic systems [27]–[31]. To obtain the CARIMA model of the parafoil system, we know its parameters are self-learning online by a selective recursive least square method, which is robust and avoid the data being saturated.

The heading of the parafoil system is expressed by:

$$\psi(k) = \varphi^T(k)\theta + \zeta(k). \tag{18}$$

$$\theta = [a_1, \cdots, a_{n_a}, b_0, \cdots, b_{n_b}]^T. \tag{19}$$

$$\varphi(k) = \begin{bmatrix} -\Delta\psi(k-1), \cdots, -\Delta\psi(k-n_a), \\ \Delta u(k-1), \cdots, \Delta u(k-n_b-1)]^T \end{bmatrix}. \tag{20}$$

$$\Delta\psi(k-i) = \psi(k-i) - \psi(k-i-1), \quad i = 1, \cdots, n_a. \tag{21}$$

$$\Delta u(k-j) = u(k-j) - u(k-j-1), \quad j = 1, \cdots, n_b. \tag{22}$$

where n_a and n_b are the number of orders need to identify. $\psi(k-i)$ denotes the heading angle of the parafoil system at $(k-i)$-th sample time, and $u(k-j)$ denotes the unilateral deflection of its trailing edge at $(k-i)$-th sample time.

The recursive least squares method with forgetting factor λ is adopted to estimate parameters of the system:

$$\begin{cases} \hat{\theta}(k) = \hat{\theta}(k-1) + K(k)[-\Delta\psi(k) - \varphi^T(k)\hat{\theta}(k-1)] \\ K(k) = P(k-1)\varphi(k)[\varphi^T(k)P(k-1)\varphi(k) + \lambda]^{-1} \\ P(k) = \lambda^{-1}[1 - K(k)\varphi^T(k)]P(k-1) \end{cases} \tag{23}$$

Substitute $\hat{\theta}(k)$ for $\theta(k)$, the CARIMA model of the parafoil system yields to:

$$A(z^{-1})y(k) = B(z^{-1})u(k-1) + C(z^{-1})\xi(k)/\Delta. \tag{24}$$

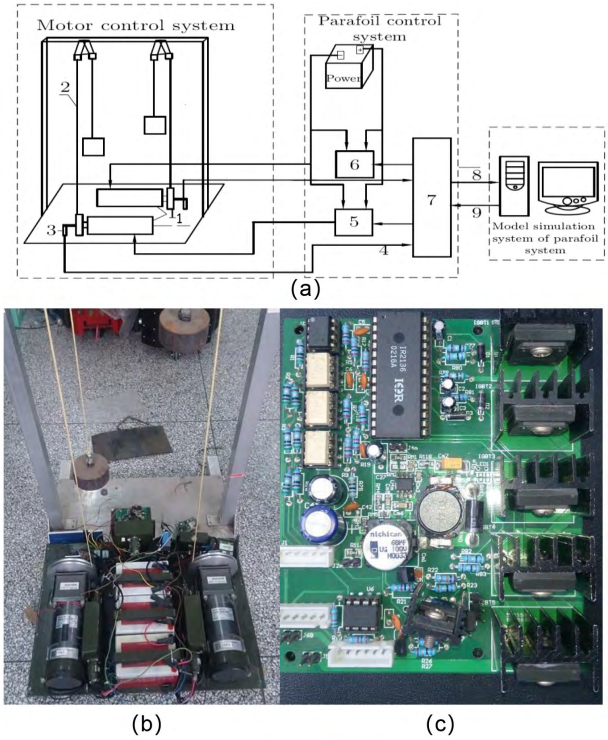

FIGURE 6. Semi-physical simulation platform. (a) The structure diagram. (b) Motor control system. (c) Driving circuit board.

where $y(k)$ is the measured output of the system, $u(k)$ is the control input and $\xi(k)$ is the uncorrelated random noise sequence, $\Delta = 1 - z^{-1}$ denotes the differential operator, $A\left(Z^{-1}\right)$, $B\left(Z^{-1}\right)$ and $C\left(Z^{-1}\right)$ are polynomials of order n_a, n_b and n_c, respectively, which are given by:

$$\begin{cases} A(z^{-1}) = 1 + a_1 z^{-1} + \cdots + a_{n_a} z^{-n_a} \\ B(z^{-1}) = b_0 + b_1 z^{-1} + \cdots + b_{n_b} z^{-n_b} \\ C(z^{-1}) = 1 + c_1 z^{-1} + \cdots + c_{n_c} z^{-n_c} \end{cases} \tag{25}$$

where a_i, b_i and c_i are coefficients of $A\left(Z^{-1}\right)$, $B\left(Z^{-1}\right)$ and $C\left(Z^{-1}\right)$, respectively.

In order to improve the robustness of the system, ψ_r is uaually softened by the one order lag model:

$$\begin{cases} \psi_r(k) = \psi(k) \\ \psi_r(k+j) = \alpha^j\psi(k) + (1-\alpha^j)\psi_r \quad (j = 1, \cdots, N) \end{cases} \tag{26}$$

where α denotes the softness factor.

According to the solution procedure of GPC [25]–[31], predictive control data $u(k)$, equivalent to the flaps deflection angle, can be calculated by employing rolling optimization every sample time. Considering flight stability of the parafoil system, $u(k)$ is needed to do a certain amplitude limit.

IV. SIMULATION EXAMPLES

A. SEMI-PHYSICAL SIMULATION PLATFORM

The simulation is divorced from the actual airdrop environment absolutely, which is only limited to computer and too idealistic. And the airdrop experiment has disadvantages of high cost, significant risk and long period. Here, we introduce

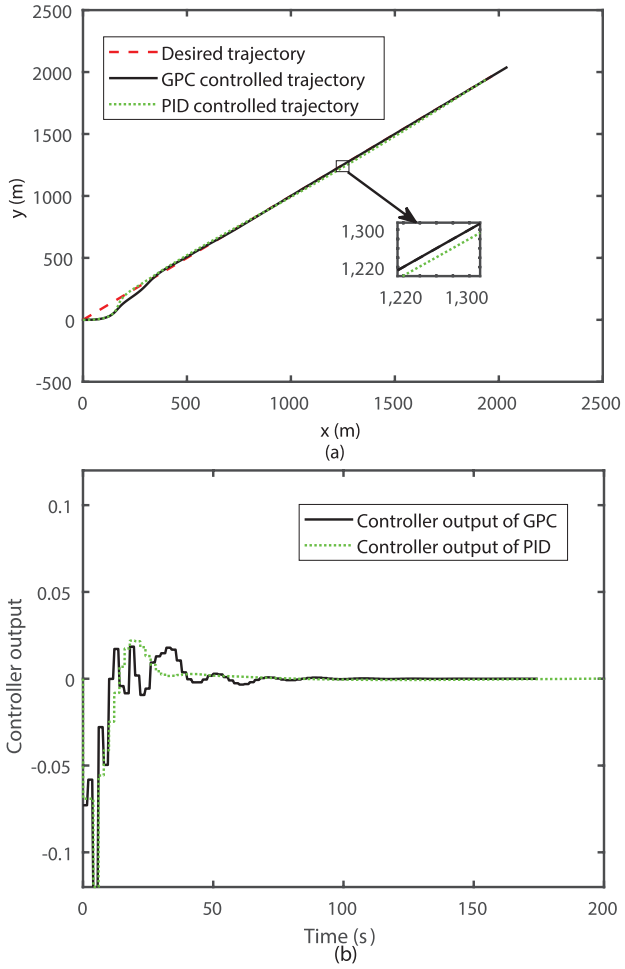

FIGURE 7. Following a line controlled by PID and GPC. (a) Controlled and designed trajectory. (b) Control quantities.

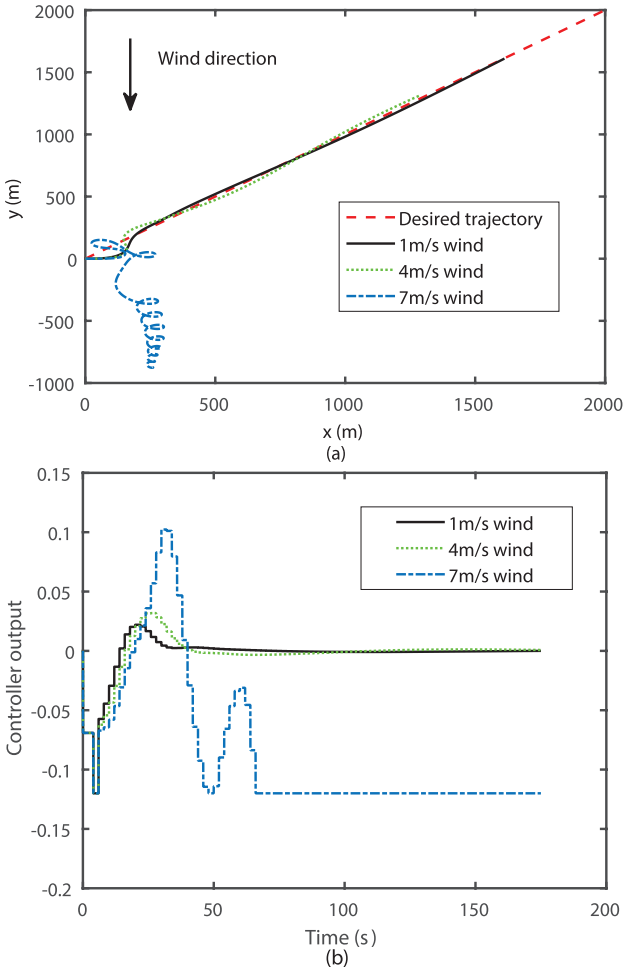

FIGURE 8. PID controlled line following in winds. (a) Horizontal trajectories. (b) Control quantities.

the semi-physical simulation platform [32], [33], combining the nonlinear dynamic model of a parafoil system with the actual components of a controller and motors, to test path following methods of the parafoil system.

The semi-physical simulation platform is mainly composed of the model simulation system of the parafoil system, the parafoil control system, and the motor control system. As shown in Fig.6 (a), the motor control system mainly consists of left and right motors (1), which are used to stretch out and pull back the steering ropes (2). Meanwhile, a multi-turn potentiometer (3) is equipped on each motor shaft to measure the rotation angle. The parafoil control system is constituted by a power plant, two motor drivers (5 and 6) and a controller (7). The model simulation system is composed of a computer and application software based on Matlab. Fig.6(b) and (c) shows the actual photo of the motor control system and the driving circuit board of the semi-physical simulation system.

For a practical parafoil system, the geographical information is collected by GPS modules. To realize the seamless connection of the model simulation system and the parafoil control system, we apply the inverse transformation of the Gauss-Kruger projection method to transform position information in Cartesian coordinates into GPS information format.

The parameters of the simulation model of the parafoil system are set the same as listed in Table 1. The initial values of motion are set as follows: initial velocity $[u, v, w]^T = [15.9, 0, 2.1]^T$, initial Euler angles $[\xi, \theta, \Psi]^T = [0, 0, 0]^T$, initial angular velocity $[p, q, r]^T = [0, 0, 0]^T$. According to the actual GPS sampling period (4HZ) and the time required for one revolution of motors (1.5s/circle), the control circle is set as 2 s.

To verify the path following control performance, both GPC and PID controllers are applied for horizontal path following. Parameters of the CARIMA model identification are set as: $n_a = 3, n_b = 5$. The GPC parameters are set as: $N = 6$, $N_u = 1$, $\lambda = 1$, $\alpha = 0.1$. The PID controller parameters are set as: $k_p = -0.068$, $k_d = -0.15$, $k_i = -0.01$.

B. RESLUTS

1) TRACKING A LINE

The desired path represents a straight line in the horizontal plane, with a starting point (0, 0) and ending point (2000 m, 2000 m), shown as the red line in Fig.7 (a).

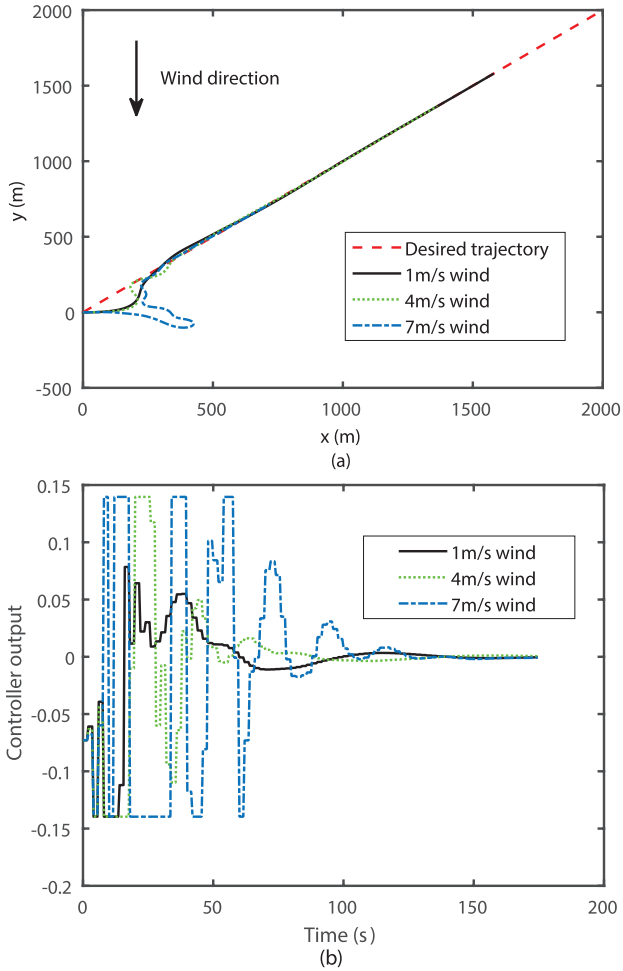

FIGURE 9. GPC controlled line following in winds. (a) Horizontal trajectories. (b) Control quantities.

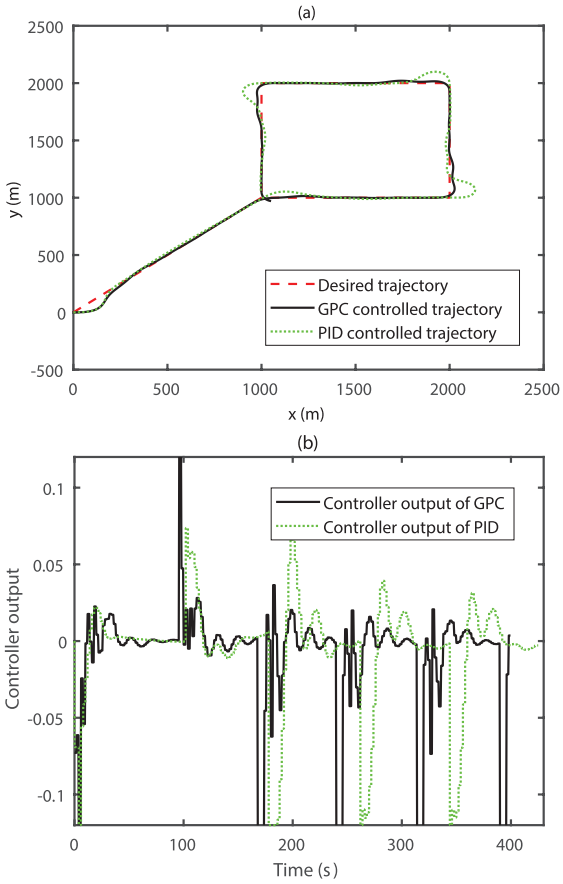

FIGURE 10. Following a rectangle controlled by PID and GPC. (a) Controlled and designed trajectory. (b) Control quantities.

A comparison between GPC and traditional PID controllers is presented in Fig.7.

We can see that both GPC and PID controllers can track the desired line well. Because of the inertia of the parafoil system, control quantities reach the maximum after the vehicle leaves the starting point. As the vehicle begins approaching the line, the control quantity becomes larger, the dominant error is the course deviation. When the vehicle closes to the line, the control quantity is small, the dominant error is the position deviation. The parafoil system eventually tracks the desired path by adjusting the heading angle continuously. However, the significant difference of control performances between GPC and PID controllers lies in the error oscillation, even though the settling time of GPC and PID controllers are similar, the GPC controller outperforms PID controller with smaller error vibration amplitude.

As introduced in former sections, the parafoil system is a kind of low-speed vehicle, its flight status is more susceptible to winds. Once the vehicle tracks the desired path in a windy environment, the wind is treated as the external disturbance of the whole system. Because the influences of horizontal winds on trajectory tracking of the parafoil system are the most lasting and intense, the horizontal constant wind is added to the simulated environment in this paper. Fig.8 shows the PID controlled horizontal trajectory in 1 m/s, 4 m/s and 7 m/s sustained winds. Fig.9 shows the GPC controlled horizontal trajectory in 1 m/s, 4 m/s and 7 m/s sustained winds, and Fig.13 shows the corresponding control quantities. For the PID controller, when the wind speed increases to 7 m/s, the whole system will lose stability, such that the parafoil system cannot perform the tracking task successfully. Whereas, the GPC controller can resist the wind up to 7 m/s, although there appears a larger error deviation at the beginning, which shows strong anti-disturbance performance and robustness of GPC. It is obvious that the control quantities increase with winds, so as to work against wind resistance, and after a period, the tracking trajectory converges to the desired path timely.

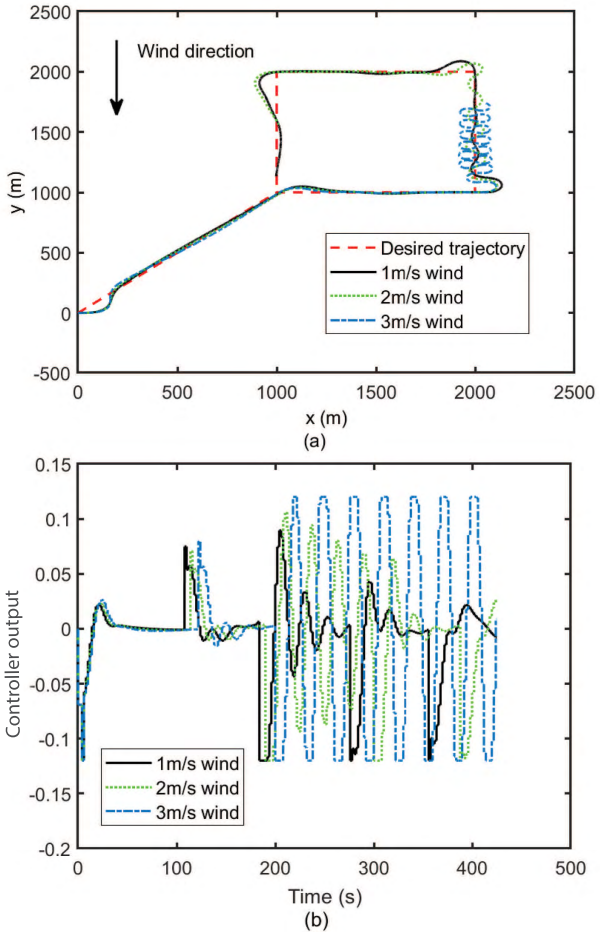

FIGURE 11. PID controlled rectangle following in winds. (a) Horizontal trajectories. (b) Control quantities.

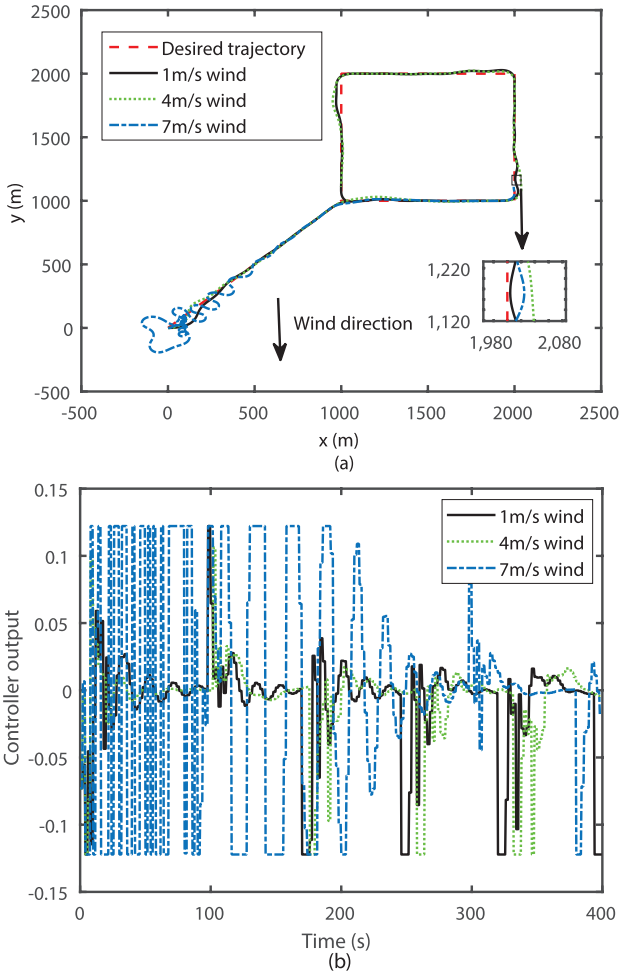

FIGURE 12. GPC controlled rectangle following in winds. (a) Horizontal trajectories. (b) Control quantities.

2) TRACKING A RECTANGLE

The desired path is a counterclockwise rectangle with four vertices (1000 m, 1000 m), (2000 m, 1000 m), (2000 m, 2000 m) and (1000 m, 2000 m), a short horizontal straight line from (0, 0) is added to the rectangle for the parafoil system to glide steadily before tracks the rectangle, which is shown as the red line in Fig.10 (a). A comparison between GPC and traditional PID controllers is presented in Fig.10.

We can observe that GPC and PID controllers still can do a good job when tracking a square shape with a 1000 m side, even with the 90° right-angle bends. As shown in Fig.10 (a), both the GPC and PID controllers have a similar distance overshoot when it tracks the line, but when the parafoil system turns right at the first corner, the performance revealed more significant differences. The distance error of GPC vibrates in a smaller range than that of PID controller, especially at intersections. Shown as Fig.10 (b), the corresponding control quantities becomes larger when the vehicle turns. And compared with the PID controller, the GPC can able to predict both the future path and control sequences to achieve the desired outcome.

The same as before, the horizontal constant wind fields are taken into consideration. Fig.11 shows the PID controlled horizontal trajectory in 1 m/s, 2 m/s and 3 m/s sustained winds. Fig.12 shows the GPC controlled horizontal trajectory in 1 m/s, 4 m/s and 7 m/s sustained winds. For the PID controller, it cannot resist 3m/s constant wind disturbance for the complexity of the desired tracking trajectory. However, when the wind speed increases up to 7 m/s, the GPC controller still can track the desired rectangle path, even though the vehicle turns several rounds nearby the starting point. We can still observe that the control quantity increases accordingly with the wind speed to resist the wind disturbances.

For performing more intuitive analyses of posture changes of the parafoil system in the trajectory tracking process, the gliding ratio and Euler angles of the vehicle are depicted by Fig. 13 under the situation of tracking the rectangle with the 4 m/s wind.

From Fig.13, we could draw a conclusion that the horizontal velocity and total resultant velocity are remained unchanged during the tracking process, which is very different from uncontrolled circumstances. The velocity of the

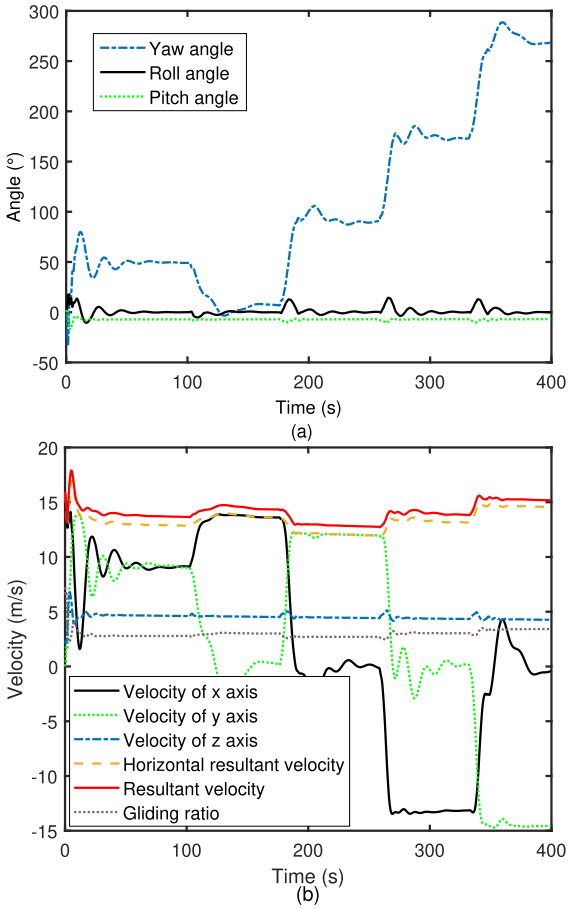

FIGURE 13. Posture changes of the parafoil system. (a) The variation of velocities and gliding ratio. (b) The obtained Euler angles.

z-axis, the roll and pitch angles are stable within a certain range to show the stability of the parafoil system in the process of trajectory tracking.

V. CONCLUSION

By using CFD simulation, we analyzed the aerodynamic performance of the parafoil system in windy conditions. Also, we obtained the equivalent force and action point of winds by performing simulation analysis. Based on that, we developed the six DoF dynamic model of the parafoil system in the wind environment. Considering the problem of nonlinear, large inertial existed in the system and strong disturbances in the airdrop environment, we came up with a novel method for autonomous path following control of the parafoil system based on GPC. Through online identification, the underlying CARIMA model was established for the motor control input and the actual output. Then the GPC strategy was used for calculating the control quantity of the desired heading angle. At last, a semi-physical simulation platform was introduced to verify the path following control of the parafoil system. The achieved simulation results demonstrate that GPC is efficient to control the parafoil system tracking desired trajectories, regardless of wind disturbances. Also, our study reveals that the method possesses better dynamic performance and much better anti-wind ability compared to traditional PID strategy. This indicates that GPC is a simple, effective strategy for trajectory tracking control of parafoil systems.

As future work, we would like to improve the accuracy of the model in windy environments, the control effects, and evaluate the controllers in the actual parafoil system. We believe that such a study will complement existing work in this area and also the results will be highly beneficial when it comes to practical applications.

REFERENCES

[1] O. A. Yakimenk, "Precision aerial delivery systems: Modeling, dynamics, and control," *Proc. AIAA*, Reston, VA, USA, Jan. 2015, pp. 123–135.

[2] R. Benney, J. Barber, J. McGrath, J. McHugh, G. Noetscher, and S. Tavan, "The new military applications of precision airdrop systems," in *Proc. Infotech Aerospace Conf.*, Reston, VA, USA, 2005, p. 7069.

[3] J. Xiong, "Research on the dynamics and homing project of parafoil system," Ph.D. dissertation, Dept. School Aerosp. Mater. Eng., Nat. Univ. Defense Technol., Changsha, China, 2005.

[4] J. Tao, Q.-L. Sun, Z.-Q. Chen, and Y.-P. He, "NSGAII based multi-objective homing trajectory planning of parafoil system," *J. Cent. South Univ.*, vol. 23, no. 12, pp. 3248–3255, Jan. 2017. doi: 10.1007/s11771-016-3390-8.

[5] L. M. Zhang, H. T. Gao, Z. Chen, Q. Sun, and X. Zhang, "Multi-objective global optimal parafoil homing trajectory optimization via Gauss pseudospectral method," *Nonlinear Dyn.*, vol. 72, nos. 1–2, pp. 1–8, 2013. doi: 10.1007/s11071-012-0586-9.

[6] T. M. Barrows, "Apparent mass of parafoils with spanwise camber," *J. Aircr.*, vol. 39, no. 3, pp. 445–451, 2002. doi: 10.2514/2.2949.

[7] P. A. Mortaloni, O. A. Yakimenko, V. N. Dobrokhodov, and R. M. Howard, "On the development of six-degree-of-freedom model of low-aspect-ratio parafoildelivery system," in *Proc. 17th AIAA Aerodyn. Decelerator Syst. Technol. Conf. Seminar*, Reston, VA, USA, 2003, p. 2105.

[8] E. Zhu, Q. Sun, P. Tan, Z. Chen, X. Kang, and Y. He, "Modeling of powered parafoil based on kirchhoff motion equation," *Nonlinear Dyn.*, vol. 79, no. 1, pp. 617–629, Oct. 2014. doi: 10.1007/s11071-014-1690-9.

[9] O. Yakimenko, "On the development of a scalable 8-DoF model of a generic parafoil-based delivery system," in *Proc. 18th AIAA Aerodynamic Decelerator Syst. Technol. Conf. Seminar*, Reston, VA, USA, 2005, p. 1665.

[10] E. Mooij, Q. Wijnand, and B. Schat, "9 DoF parafoil/payload simulator development and validation," in *Proc. AIAA Modeling Simulation Technol. Conf. Seminar*, Reston, VA, USA, 2003, p. 5459.

[11] Y. Ochi and M. Watanabe, "Modelling and simulation of the dynamics of a powered paraglider," *Proc. Inst. Mech. Eng. G, J. Aerosp. Eng.*, vol. 225, no. 4, pp. 373–386, Apr. 2011. doi: 10.1177/09544100JAERO888.

[12] N. Slegers and M. Costello, "Model predictive control of a parafoil and payload system," *J. Guid., Control, Dyn.*, vol. 28, no. 4, pp. 816–821, 2005. doi: 10.2514/1.12251.

[13] O. Prakash and N. Ananthkrishnan, "Modeling and simulation of 9-DOF parafoil-payload system flight dynamics," in *Proc. AIAA Atmospheric Flight Mech. Conf. Exhibit*, Reston, VA, USA, 2006, p. 6130.

[14] L. Jiao, Q. Sun, X. Kang, Z. Chen, and Z. Liu, "Autonomous homing of parafoil and payload system based on ADRC," *J. Control. Eng. Appl. Inf.*, vol. 13, no. 3, pp. 25–31, 2011.

[15] J. Tao, Q. Sun, H. Sun, Z. Chen, M. Dehmer, and M. Sun, "Dynamic modeling and trajectory tracking control of parafoil system in wind environments," *IEEE-ASME Trans. Mechatron.*, vol. 22, no. 6, pp. 2736–2745, Dec. 2017. doi: 10.1109/TMECH.2017.2766882.

[16] J. Tao, Q. Sun, P. Tan, Z. Chen, and Y. He, "Active disturbance rejection control (ADRC)-based autonomous homing control of powered parafoils," *Nonlinear Dyn.*, vol. 86, no. 3, pp. 1461–1476, 2016. doi: 10.1007/s11071-016-2972-1.

[17] S. Luo *et al.*, "On decoupling trajectory tracking control of unmanned powered parafoil using ADRC-based coupling analysis and dynamic feedforward compensation," *Nonlinear Dyn.*, vol. 92, no. 4, pp. 1619–1635, Jun. 2018. doi: 10.1007/s11071-018-4150-0.

[18] T. Jann,"Advanced features for autonomous parafoil guidance, navigation and control," in *Proc. 18th AIAA Aerodynamic Decelerator Syst. Technol. Conf. Seminar*, Reston, VA, USA, 2005, p. 1642.

[19] I. I. Kaminer and O. A. Yakimenko, "On the development of GNC algorithm for a high-glide payload delivery system," in *Proc. 42nd IEEE Int. Conf. Decision Control*, Maui, HI, USA, Dec. 2003, pp. 5438–5443.
[20] K. J. Åström and T. Hägglund, *PID Controllers: Theory, Design, and Tuning*, vol. 2. Raleigh, NC, USA: Research Triangle Park, 1995, pp. 5–9.
[21] Y. Kang and J. K. Hedrick, "Linear tracking for a fixed-wing UAV using nonlinear model predictive control," *IEEE Trans. Control Syst. Technol.*, vol. 17, no. 5, pp. 1202–1210, Apr. 2009. doi: 10.1109/TCST.2008.2004878.
[22] J. Thongsri, "A successful CFD-based solution to a water condensation problem in a hard disk drive factory," *IEEE Access*, vol. 5, pp. 10795–10804, 2017. doi: 10.1109/ACCESS.2017.2708138.
[23] S. Nategh, Z. Huang, A. Krings, O. Wallmark, and M. Leksell, "Thermal modeling of directly cooled electric machines using lumped parameter and limited CFD analysis," *IEEE Trans. Energy Convers.*, vol. 28, no. 4, pp. 979–990, Dec. 2013.
[24] A. Eslambolchi and H. Johari, "Simulation of flowfield around a ram-air personnel parachute canopy," *J. Aircr.*, vol. 50, no. 5, pp. 1628–1636, 2014. doi: 10.2514/1.C032169.
[25] D. Clarke, C. Mohtadi, and P. Tuffs, "Generalized predictive control—Part I. The basic algorithm," *Automatica*, vol. 23, no. 2, pp. 137–148, Mar. 1987. doi: 10.1016/0005-1098(87)90087-2.
[26] D. W. Clarke, C. Mohtadi, and P. S. Tuffs, "Generalized predictive control—Part II extensions and interpretations," *Automatica*, vol. 23, no. 2, pp. 149–160, Mar. 1987. doi: 10.1016/0005-1098(87)90088-4.
[27] J. Rawlings, "Tutorial overview of model predictive control," *IEEE Control Syst. Mag.*, vol. 20, no. 3, pp. 38–52, Jun. 2000. doi: 10.1109/37.845037.
[28] X. Zhang, T. Shi, Z. Wang, Q. Geng and C. Xia, "Generalized predictive contour control of the biaxial motion system," *IEEE Trans. Ind. Electron.*, vol. 65, no. 11, pp. 8488–8497, Nov. 2018. doi: 10.1109/TIE.2018.2808899.
[29] J. Castelló, J. M. Espí, and R. García-Gil, "A new generalized robust predictive current control for grid-connected inverters compensates anti-aliasing filters delay," *IEEE Trans. Ind. Electron.*, vol. 63, no. 7, pp. 4485–4494, Jul. 2016, doi: 10.1109/TIE.2015.2497303.
[30] W. J. He *et al.*, "Generalized predictive control of temperature on an atomic layer deposition reactor," *IEEE Trans. Control Syst. Technol.*, vol. 23, no. 6, pp. 2408–2415, Nov. 2015. doi: 10.1109/TCST.2015.2404898.
[31] S. Wen, J. Zhu, X. Li, and S. Chen, "A double-loop structure in the adaptive generalized predictive control algorithm for control of robot end-point contact force," *ISA Trans.*, vol. 53, no. 5, pp. 1603–1608, Sep. 2014.
[32] G. Hai-Tao, Y. Sheng-Bo, Z. Er-Lin, S. Qing-Lin, C. Zeng-Qiang, and K. Xiao-Feng, "Semi-physical simulation platform of a parafoil nonlinear dynamic system," *Chin. Phys. Lett.*, vol. 30, no. 11, 2013, Art. no. 110503. doi: 10.1088/0256-307X/30/11/110503.
[33] Q. L. Sun, L. Jiao, Z. Q. Chen, T. L. Wu, and X. J. Zou, "Parafoil autonomous homing semi-physical simulation system," China Patent 10 232 375 9B, Mar. 6, 2013.

JIN TAO received the B.Sc. degree in automation from the Qingdao University of Science and Technology, Qingdao, China, in 2008, the M.Sc. degree in control theory and control engineering from the Guangxi University of Science and Technology, Liuzhou, China, in 2011, and the Ph.D. degree in control science and engineering from Nankai University, Tianjin, China, in 2017. From 2010 to 2011, he spent two years as a joint Training Student with the Intelligent Control Laboratory, College of Engineering, Peking University, Beijing, China. From 2011 to 2014, he was a Chief Engineer with the Institute of Rotary Drilling Machine, Beijing Sany Heavy Machinery Co., Ltd., Beijing.

He is currently an Academy of Finland Postdoctoral Researcher with Aalto University, Espoo, Finland. He is also with the College of Engineering, Peking University. He has published more than 30 peer-reviewed papers in international journals and conferences. His research interests include advanced control, evolutionary optimization, dynamic modeling, and their applications.

MATTHIAS DEHMER received the B.Sc. degree in mathematics from the University of Siegen, Germany, in 1997, and the Ph.D. degree in computer science from the Darmstadt University of Technology, Germany, in 2005.

He is currently a Professor with the University of Applied Sciences Upper Austria, Campus Steyr. He is also with UMIT—The Health and Life Sciences University, Hall in Tyrol, Austria, and also with Nankai University, Tianjin, China. He has authored and coauthored more than 245 publications. His h-index equals 33 and his i10-index equals 101. His research interests include data science, cybersecurity, disaster management, complex networks, risk analysis, information systems, machine learning, information theory, bioinformatics, visual analytics, and computational statistics.

GUANGMING XIE (M'12) received the B.S. degree in applied mathematics and electronic and computer technology, the M.E. degree in control theory and control engineering, and the Ph.D. degree in control theory and control engineering from Tsinghua University, Beijing, China, in 1996, 1998, and 2001, respectively.

From 2001 to 2003, he was a Postdoctoral Research Fellow with the Center for Systems and Control, Department of Mechanics and Engineering Science, Peking University, Beijing, China. In 2003, he joined the Center as a Lecturer. He is currently a Full Professor of dynamics and control with the College of Engineering, Peking University. His research interests include smart swarm theory, multiagent systems, multirobot cooperation, biomimetic robot, switched and hybrid systems, and networked control systems.

Dr. Xie is an Associate Editor of *Scienti?c Reports*, the *International Journal of Advanced Robotic Systems*, *Mathematical Problems in Engineering*, and an Editorial Board Member of the *Journal of Information and Systems Science*.

QUAN ZHOU (M'02) received the M.Sc. and Dr. Tech. degrees from the Tampere University of Technology, Finland. He was a Professor with Northwest Polytechnical University, Xi'an, China. He is currently an Associate Professor with the Robotic Instruments Group, School of Electrical Engineering, Aalto University, Finland. His work has been published in major international journals, including *Nature Communications*, *Advanced Materials*, *Small*, and the IEEE TRANSACTIONS ON ROBOTICS. His current research interests include micro and nano manipulation, and automation methods. He was a recipient of the Anton Paar Research Award for Instrumental Analytics and Characterization. He was also the Chair of the IEEE Finland Joint Chapter of Control System Society, the Robotics and Automation Society, and the System Man and Cybernetics Society. He is also serving as a Topic Editor-in-Chief for the *International Journal of Advanced Robotic Systems*, a member of Editorial Board of the *Journal of Micro-Bio Robotics*, and was an Associate Editor/Guest Editors of several other journals. He was the coordinator of EU FP7 project FAB2ASM, the first PPP Project of the European Economic Recovery Plan.